

Electroreflectance lineshapes in multilayered semiconductor structures: Influence of the linear electro-optic effect

Jayeeta Bhattacharyya, Sandip Ghosh,^{*} and B. M. Arora

*Department of Condensed Matter Physics and Material Science, Tata Institute of Fundamental Research,
Homi Bhabha Road, Mumbai 400005, India*

T. J. C. Hosea

Department of Physics, University of Surrey Guildford, Surrey GU2 7XH, United Kingdom

(Received 9 September 2008; revised manuscript received 16 October 2008; published 13 November 2008)

The authors report the observation of strongly polarization-sensitive resonances in the electroreflectance (ER) spectra of multilayered semiconductor structures. The measurements were done on vertical-cavity surface-emitting laser structures grown on GaAs(001) substrates. The ER spectral features undergo a 180° phase shift as the polarization vector \mathbf{E} of the probe beam is rotated by 90° from $E_{\parallel}[\bar{1}\bar{1}0]$ to $E_{\parallel}[110]$ in the (001) plane. Through experiments and simulations, these resonances are shown to arise due to the linear electro-optic effect (LEOE). The influence of LEOE at energies below the band gap becomes prominent mainly because of optical-interference induced enhancement of the Seraphin coefficients in a multilayered structure. Implications for the analysis of ER spectral lineshapes of multilayered semiconductor structures are highlighted.

DOI: [10.1103/PhysRevB.78.195312](https://doi.org/10.1103/PhysRevB.78.195312)

PACS number(s): 78.20.Jq, 78.20.Bh, 78.66.Fd, 78.40.Fy

I. INTRODUCTION

Electric-field modulated spectroscopy techniques such as electroreflectance (ER) and photorefectance (PR) are important tools for studying the electronic band structure (EBS) of semiconductors, especially low-dimensional structures such as quantum wells (QWs), and for characterizing devices based on them.^{1,2} In ER/PR, one measures the change in the reflectance of the semiconductor due to an electric-field induced change in its dielectric function. A typical spectrum has sharp resonant features at photon energies close to van Hove singularities, also called critical points, in the EBS of the semiconductor sample where the modification of the dielectric function is most prominent.³ Information about the critical points, and thereby the EBS, is obtained through an analysis of the spectral lineshapes. Consequently, it is crucial to be able to identify the physical mechanisms of dielectric function change that lead to the intricate ER/PR lineshapes. In the literature, the following are the most commonly invoked mechanisms of dielectric function change due to the application of an electric field. In the case of bulk semiconductors, the acceleration of free charge carriers leads to a dielectric function change, referred to as the Franz-Keldysh effect (FKE).⁴ For carriers bound by a Coulomb potential, that is, excitons, field-induced ionization results in a dielectric function modification.⁵ In the case of QWs, the application of an electric field along the confinement direction cannot accelerate free charges nor ionize excitons. Instead, a modification of the confinement potential leads to a redshift of the interband transition energies, referred to as the quantum-confined Stark effect (QCSE), which in turn affects the dielectric function.⁶ The modification of the dielectric function due to all the above mechanisms has a quadratic dependence on the electric field and is independent of the linear polarization state of a probe beam incident normally on the surface.

In this paper, we show that the linear electro-optic effect (LEOE) can also give rise to very sharp resonant features in the ER spectrum of multilayered structures. LEOE arises in crystals lacking a center of inversion symmetry and is associated with field-induced displacements of positive and negative ions in opposite directions.⁷ We explain why the influence of LEOE, which is normally ignored in ER lineshape analysis, becomes prominent in the case of multilayered structures. Modern semiconductor optoelectronic devices often have a multilayered structure, and for these experiments we have used as-grown vertical-cavity surface-emitting laser (VCSEL) device structures. A VCSEL consists of QWs in the active region and a thin cavity that is sandwiched between a top and a bottom distributed Bragg reflector (DBR).⁸ The cavity supports a single cavity mode (wavelength λ_{CM}) over the whole gain spectrum. Such structures typically have several epitaxially grown layers. Apart from the basic issue related to understanding the origins of ER lineshapes in multilayered structures, this study is also of practical importance for postgrowth characterization of VCSEL structures. An important such characterization step involves estimating the wavelength positions of the ground-state transition in the QW active region (λ_{QW}) and λ_{CM} . The coincidence of λ_{QW} and λ_{CM} at the working temperature is essential for efficient device operation.⁹ Nondestructive estimation of λ_{QW} is extremely challenging because optical interference in the DBRs hinders photoluminescence measurements typically used to determine λ_{QW} .⁸ ER and PR have been more promising in this regard; it has been shown that the change in the amplitude¹⁰ or the symmetry^{11,12} of the ER/PR lineshape around λ_{CM} , as λ_{QW} and λ_{CM} are brought into coincidence by various means, can be used to determine λ_{QW} . Thus an understanding of the different origins of ER lineshapes in VCSEL structures is crucial for the application of ER to VCSEL characterization. This study tries to bring out the importance of recognizing these LEOE-related ER reso-

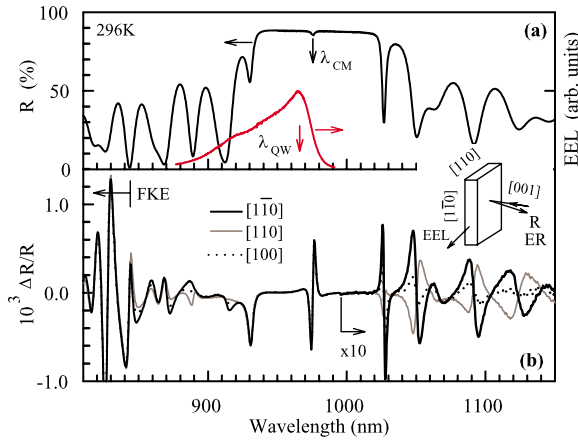


FIG. 1. (Color online) (a) Reflectance $R(\lambda)$ and EEL spectrum of VCSEL#1 at room temperature. (b) Its ER spectra for different polarizations of the probe. The schematic shows the measurement geometry for R, ER, and EEL, and indicates that $[1\bar{1}0]$ and $[110]$ are parallel to the cleaved sample edges.

nances and the implications for both measurement and interpretation of ER spectra of multilayered semiconductor structures/devices in general.

II. EXPERIMENTAL DETAILS

The two VCSEL structures used in this study were grown using metal-organic vapor-phase epitaxy on n^+ -GaAs(001) substrates. VCSEL#1 was designed for infrared emission and has doped $\text{Al}_{0.15}\text{Ga}_{0.85}\text{As}/\text{Al}_{0.95}\text{Ga}_{0.05}\text{As}$ (26 p -doped top pairs, 13 n -doped bottom pairs) DBRs, undoped cavity of $\text{Al}_{0.18}\text{Ga}_{0.82}\text{As}$, and five $\text{In}_{0.16}\text{Ga}_{0.84}\text{As}/\text{GaAs}_{0.95}\text{P}_{0.05}$ QWs which form the active region. VCSEL#2 was designed for visible emission and has doped $\text{Al}_{0.6}\text{Ga}_{0.4}\text{As}/\text{Al}_{0.95}\text{Ga}_{0.05}\text{As}$ (41 p -doped top pairs, 63 n -doped bottom pairs) DBRs, undoped cavity of $(\text{Al}_{0.7}\text{Ga}_{0.3})_{0.52}\text{In}_{0.48}\text{P}$, and four $\text{Ga}_{0.42}\text{In}_{0.58}\text{P}/(\text{Al}_{0.3}\text{Ga}_{0.7})_{0.52}\text{In}_{0.48}\text{P}$ QWs as the active region. ER measurements were done in the soft-contact mode¹³ with the sample sandwiched between a flat copper electrode and a transparent conducting indium-tin-oxide coated glass acting as the second electrode. A modulation voltage of $0.71 V_{\text{rms}}$ at a frequency $f_m = 175 \text{ Hz}$ with a -1 V bias was used in the measurements. For the probe beam, light from a 100 W tungsten lamp was dispersed by a monochromator (0.8 nm band pass) and then linearly polarized with a Glan-Taylor polarizer. A quartz wedge depolarizer was used for measurements requiring unpolarized light. Si and InGaAs photodiodes were used along with a lock-in amplifier for detection. To independently estimate λ_{QW} we also measured the edge electroluminescence (EEL) spectrum emerging through the sides of a cleaved wafer, thereby avoiding DBR-related spectral distortions.¹⁴

III. RESULTS AND DISCUSSIONS

Figure 1(a) shows the unpolarized reflectance $[R(\lambda)]$ spectrum of VCSEL#1 ($\theta_{\text{incidence}} \sim 13^\circ$), where the dip in the high reflectance band identifies λ_{CM} . The peak of the EEL

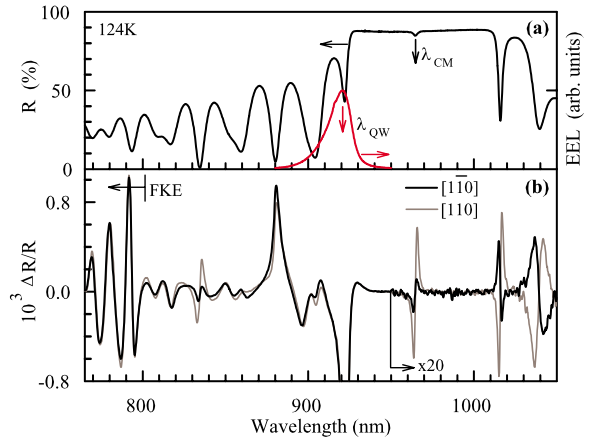


FIG. 2. (Color online) (a) Reflectance $R(\lambda)$ and EEL spectrum of VCSEL#1 at low temperature. (b) Its low-temperature electroreflectance spectra for probe beam polarization $E \parallel [1\bar{1}0]$ and $E \parallel [110]$.

spectrum, also shown in Fig. 1(a), identifies λ_{QW} . The ER spectra of VCSEL#1 for probe beams that are linearly polarized along $E \parallel [1\bar{1}0]$ and $E \parallel [110]$ are shown in Fig. 1(b). The ER signal can be expressed as

$$\Delta R/R(\lambda) = \alpha(\lambda)\Delta\epsilon_1(\lambda) + \beta(\lambda)\Delta\epsilon_2(\lambda), \quad (1)$$

where $\alpha(\lambda) = R(\lambda)^{-1}[\partial R(\lambda)/\partial\epsilon_1]$ and $\beta(\lambda) = R(\lambda)^{-1}[\partial R(\lambda)/\partial\epsilon_2]$ are the Seraphin coefficients. ER resonances are commonly understood as arising from structure in electric-field-induced change $\Delta\epsilon_{1,2}(\lambda)$ in the complex dielectric function $[\epsilon_1 + i\epsilon_2]$, with $\alpha(\lambda)$ and $\beta(\lambda)$ being slowly varying functions of λ . The ER spectrum of VCSEL#1 has many sharp resonances which we classify into three groups. In group (i) below 850 nm, the features originate mainly due to structure in $\Delta\epsilon_{1,2}(\lambda)$ arising from FKE in $\text{GaAs}_{0.95}\text{P}_{0.05}$ barrier layers. In group (ii) around 975 nm, the feature is due to a combination of QCSE-induced $\Delta\epsilon_{1,2}(\lambda)$ associated with the QW exciton and optical-interference modified Seraphin coefficients for a VCSEL structure¹⁰ at λ_{CM} . It has been shown earlier¹¹ that the antisymmetry of this lineshape about its central λ indicates that λ_{QW} is close to λ_{CM} . This inference is supported by the results shown in Fig. 1(a). However the resonances in group (iii) for $\lambda > 1000 \text{ nm}$ are different. Unlike the previous two cases, these undergo a 180° phase shift as the polarization vector E of the probe beam is rotated by 90° from $E \parallel [1\bar{1}0]$ to $E \parallel [110]$ and tend to cancel for $E \parallel [100]$. Also unlike the FKE-related features, there is a simple correlation in the λ position of these polarization-sensitive features with the big dips in $R(\lambda)$. We note here that $R(\lambda)$ itself did not show any significant in-plane polarization anisotropy.

Figure 2(a) shows the $R(\lambda)$ and the EEL spectrum of VCSEL#1 at 124 K, where λ_{QW} has been considerably blue-shifted relative to λ_{CM} to around $\sim 920 \text{ nm}$ by cooling the sample. Figure 2(b) shows the polarized ER spectra at 124 K. The enhanced polarization-insensitive ER signal around $\sim 920 \text{ nm}$ is an indication of the position of λ_{QW} .¹⁰ The important thing to note here is that the ER resonance around

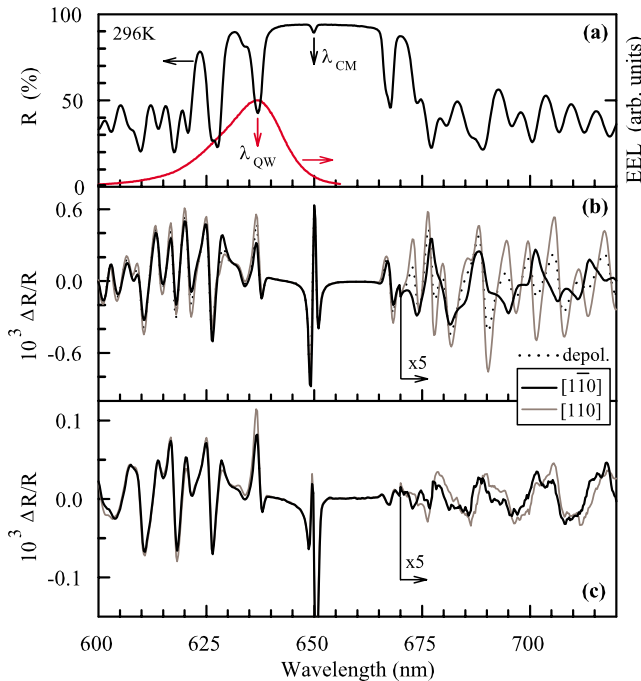


FIG. 3. (Color online) (a) Reflectance $R(\lambda)$ and EEL spectrum of VCSEL#2 at room temperature. (b) Its ER spectra for polarized and also for depolarized probe beams. (c) Polarized ER spectra measured at the second harmonic of f_m .

λ_{CM} continues to have an antisymmetric lineshape. However, unlike the room temperature spectra of Fig. 1(b), here the resonant feature around λ_{CM} shows a strong polarization anisotropy. We will show next that these polarization-sensitive features arise due to the LEOE. In the context of using ER/PR for VCSEL characterization, we can now draw the following conclusion. The antisymmetry of the ER/PR resonance around λ_{CM} is not a conclusive proof for λ_{QW} being close to λ_{CM} . It can arise even when λ_{QW} is significantly blueshifted relative to λ_{CM} and does so because of the LEOE. However the two cases may be distinguished using the fact that the LEOE-induced antisymmetric lineshape will show a strong in-plane polarization anisotropy [Fig. 2(b)] while the QCSE-induced antisymmetric lineshape, which correctly identifies the position of λ_{QW} as being close to λ_{CM} , will not [Fig. 1(b)].

In zinc-blende-type cubic semiconductor crystals, an electric field F applied along [001] gives rise to a $\Delta\epsilon_1$ LEOE $= \pm \epsilon_1^2 r_{41} F$ ($\Delta\epsilon_2$ LEOE=0) for $\lambda > \lambda_{\text{band gap}}$.^{15,16} r_{41} is the relevant electro-optic coefficient for this LEOE; its magnitude ranges between $1.0\text{--}1.5 \times 10^{-12}$ m/V in the present materials, with very weak λ dependence. The sign is positive (negative) for $E \parallel [1\bar{1}0]$ ($E \parallel [110]$), and this is the basic origin of the polarization anisotropy of these ER features which we associate with the LEOE.¹⁷ To show that such LEOE-related ER features can occur in general, we present results on a different structure (VCSEL#2) in Figs. 3(a) and 3(b). Here again one observes large in-plane polarization anisotropy in the ER resonances at longer λ . The weak anisotropy seen in the other parts of the spectrum also arise due to the LEOE. If the above explanation is correct then, for a depolarized probe

beam, the LEOE-induced features should tend to cancel. This is evident in Fig. 3(b), where the residual features seen in the spectrum with the depolarized probe beam at longer λ arise due to $\Delta\epsilon_{1,2}(\lambda)$ originating from the QCSE. The cancellation should also occur for a probe beam polarized along [100] at 45° to $E \parallel [1\bar{1}0]$ or $E \parallel [110]$, which is seen in Fig. 1(b).

As further proof for the LEOE being responsible for the occurrence of these polarization-sensitive ER resonances, we consider the following. The sample experiences an electric field of the form $F = F_o + F_m \sin(2\pi f_m t)$, where F_o accounts for the built-in field and the dc bias. The dielectric function change can in general have the form $\Delta\epsilon_i(\lambda) = l_i F + q_i F^2$ ($i = 1, 2$), where l and q are coefficients representing the linear (LEOE) and the quadratic (FKE and QCSE) field-dependent contributions. Then using Eq. (1) it is easy to show that the ER signals measured at the second harmonic ($2f_m$) of the modulation frequency will have no contribution from LEOE; instead only FKE or QCSE will contribute.¹⁸ This is clearly seen in the ER spectrum of VCSEL#2 in Fig. 3(c) recorded at $2f_m$, where now the features at longer λ are minimized and show no significant polarization anisotropy while the FKE- and QCSE-related features continue to be seen.

In order to understand fully the lineshapes of these LEOE-induced features, we have simulated the ER spectrum of VCSEL#1 at 296 K from first principles. We considered $\Delta\epsilon_1$ LEOE in all the undoped cavity region layers in which F is maximum and also $\Delta\epsilon_{1,2}(\lambda)$ due to the QCSE in the QW layers. For the QW exciton dielectric function, we adopted the Lorentz oscillator model.¹¹ The background refractive indices of the different layers were taken from literature. Then using the transfer-matrix technique¹⁹ for multilayered structures, we calculated $R(\lambda)$ for VCSEL#1 with the applied field [$\Delta\epsilon_{1,2}(\lambda)_{\text{QCSE and LEOE}} = \text{finite}$] and without it [$\Delta\epsilon_{1,2}(\lambda)_{\text{QCSE and LEOE}} = 0$]. The difference between these two reflectance spectra divided by the zero-field spectrum gave the simulated ER spectrum. The magnitude of $\Delta\epsilon_{1,2}(\lambda)$ was varied to match the simulation results with experiment. Interference effects depend on the optical path length; a product of the layer thickness (d) and the refractive index ($\sqrt{\epsilon}$). For a difference spectrum such as ER, the appropriate parameter to consider is proportional to $d\Delta\epsilon$. Figure 4(a) shows a plot of the product of the total cavity thickness ($d^{\text{cav}} = 278$ nm) and $\Delta\epsilon_1$ LEOE, along with the product of $\Delta\epsilon_{1,2}(\lambda)_{\text{QCSE}}$ and the total QW thickness ($d^{\text{QW}} = 60$ nm), representing the relative contributions of the LEOE and the QCSE over the whole spectrum. These plots show why the LEOE can usually be neglected in the analysis of conventional ER spectra; $\Delta\epsilon_1$ LEOE is typically very small compared to $\Delta\epsilon_{1,2}(\lambda)_{\text{QCSE or FKE}}$. However in a multilayered structure where optical interference has a role to play, the influence of the LEOE can be magnified by a larger layer thickness and can even become dominant at longer λ (> 1040 nm here) well below the band gap, where the influence of the FKE and the QCSE have diminished. Figure 4(b) shows the simulated $R(\lambda)$ spectrum. The simulated ER spectra in Fig. 4(c) for $E \parallel [1\bar{1}0]$ and $E \parallel [110]$ reproduce fairly well the main characteristics of the measured ER lineshapes of VCSEL#1 in Fig. 1(b), especially their polarization anisotropy at longer λ . Also shown in Fig. 4(c) is the average of the ER spectra for

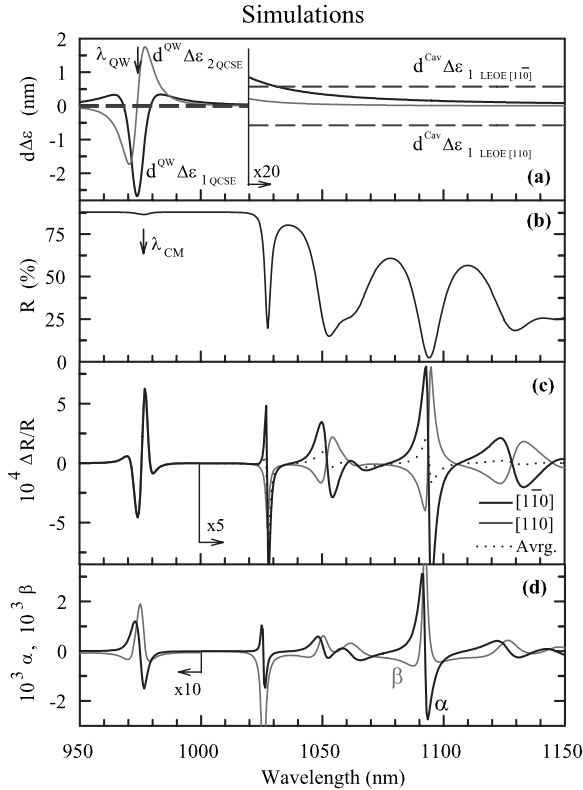


FIG. 4. (a) Calculated product of $\Delta\epsilon_{1,2}(\lambda)_{\text{QCSE}}$ with the total QW thickness d^{QW} (continuous line) and polarization-dependent $\Delta\epsilon_{1 \text{ LEOE}}$ with the total cavity thickness d^{Cav} (dashed line) in VCSEL#1. (b) Its simulated reflectance $R(\lambda)$ spectrum. (c) Its simulated electroreflectance spectra for $E||[1\bar{1}0]$, $E||[110]$, and their average. (d) Calculated Seraphin coefficients $\alpha(\lambda)$ and $\beta(\lambda)$ of VCSEL#1 for dielectric function change in a layer within the cavity region.

$E||[1\bar{1}0]$ and $E||[110]$, representing the ER spectra for $E||[100]$, $[010]$, or an unpolarized beam. We found that the LEOE-related features cancel out in the averaged spectrum and what remains is identical to the simulations when only the QCSE is considered. Again, the agreement of this simulation with the measured $E||[100]$, $[010]$ spectrum in Fig. 1(b) is satisfactory. The magnitude of $\Delta\epsilon_{1 \text{ LEOE}}$ required to match the simulations with the experiment suggests a modulation voltage of $\approx 0.2 V_{\text{rms}}$ across the cavity region. This is consistent with the applied voltage and the expected drops elsewhere in the structure, including across the contacts.¹³

We note here that a real physical process which leads to a $\Delta\epsilon$ is necessary to be able to observe an ER spectrum. In VCSEL#1 $\Delta\epsilon$ has no significant spectral structure for $\lambda > 1040$ nm. However the spectral lineshape is determined not just by the spectral structure of $\Delta\epsilon$, it also depends on

how a change in the dielectric constant affects $R(\lambda)$, which is quantified in terms of the Seraphin coefficients. Figure 4(d) shows the calculated Seraphin coefficients for VCSEL#1 for modulation of the dielectric function in a typical layer within the cavity region. The sharp resonances in the Seraphin coefficients coincide with the sharp dips in the simulated $R(\lambda)$. They arise because a small change in the dielectric constants produces a large ΔR signal wherever the optical-interference dominated $R(\lambda)$ changes rapidly with wavelength. Comparing Figs. 4(c) and 4(d), it is evident that for $\lambda > 1040$ nm the spectral lineshape of the polarization-sensitive ER resonances approximately mimic $\pm\alpha(\lambda)$. This supports our understanding that the influence of LEOE becomes observable in multilayered structures mainly because $R(\lambda)$ has sharp optical-interference-induced features which are highly sensitive to small changes in the dielectric constants of the layers. Under such circumstances the ER spectral lineshape is essentially determined by $\alpha(\lambda)$ in the region where absorption is negligible with the polarization-dependent sign of $\Delta\epsilon_{1 \text{ LEOE}}$ determining its phase. While this is consistent with Eq. (1), we note again the crucial difference from the case of ER spectra in bulk semiconductors or QWs arising from the FKE or the QCSE, respectively, where it is the structure in $\Delta\epsilon_{1,2}(\lambda)$ that determines the spectral lineshape.

In general, sharp ER spectral features due to the FKE or the QCSE enable accurate measurement of critical-point energies, which is essential for EBS-related studies on semiconductors and also postgrowth characterization of device structures. The LEOE is only expected to introduce a weak featureless background in such spectra. However the present study shows that in structures with several layers, optical-interference-induced enhancement of the Seraphin coefficients leads to a situation where even the LEOE can give rise to sharp distinct spectral features, which are also polarization sensitive. Since the light output from a monochromator is typically partially polarized, with the net polarization being λ dependent, such LEOE-related contribution to the spectrum can become unpredictable in multilayered structures. Therefore critical-point energy determination in such cases requires careful measurement and analysis. It was shown using $[001]$ -oriented cubic III-V semiconductor VCSEL structures as examples that such undesirable influence of the LEOE can be minimized if the probe beam is polarized with $E||[100]$, $[010]$, or is completely depolarized. One can also avoid it by doing measurements at the second harmonic of the electric-field modulation frequency.

ACKNOWLEDGMENT

S.G. acknowledges research grant support from the Indian National Science Academy.

*sangho10@tifr.res.in

- ¹O. J. Glembocki and B. V. Shanabrook, in *Semiconductors and Semimetals* Vol. 36, edited by D. G. Seiler and C. L. Littler (Academic, New York, 1992).
- ²F. H. Pollak and H. Shen, *Mater. Sci. Eng. R.* **10**, 275 (1993).
- ³M. Cardona, in *Solid State Physics Supp.* 11 (Academic, New York, 1969).
- ⁴D. E. Aspnes and N. Bottka, in *Semiconductors and Semimetals* Vol. 9, edited by R. K. Willardson and A. C. Beer (Academic, New York, 1972).
- ⁵D. F. Blossey, *Phys. Rev. B* **3**, 1382 (1971).
- ⁶D. A. B. Miller, D. S. Chemla, T. C. Damen, A. C. Gossard, W. Wiegmann, T. H. Wood, and C. A. Burrus, *Phys. Rev. B* **32**, 1043 (1985).
- ⁷A. Yariv, *Optical Electronics* (Saunders, Chicago, 1991).
- ⁸*Vertical-Cavity Surface-Emitting Lasers: Design, Fabrication, Characterization and Applications*, edited by C. Wilmsen, H. Temkin, and L. A. Coldren (Cambridge University Press, Cambridge, 2002).
- ⁹B. Tell, K. F. Brown-Goebeler, R. E. Leibenguth, F. M. Baez, and Y. H. Lee, *Appl. Phys. Lett.* **60**, 683 (1992).
- ¹⁰P. J. Klar, G. Rowland, P. J. S. Thomas, A. Onischenko, T. E. Sale, T. J. C. Hosea, and R. Grey, *Phys. Rev. B* **59**, 2894 (1999).
- ¹¹S. Ghosh, T. J. C. Hosea, and S. B. Constant, *Appl. Phys. Lett.* **78**, 3250 (2001).
- ¹²S. A. Choulis, T. J. C. Hosea, S. Ghosh, P. J. Klar, and M. Hofmann, *IEEE Photonics Technol. Lett.* **15**, 1026 (2003).
- ¹³S. Datta, S. Ghosh, and B. M. Arora, *Rev. Sci. Instrum.* **72**, 177 (2001).
- ¹⁴S. Ghosh, S. Constant, and T. J. C. Hosea, *J. Appl. Phys.* **88**, 1432 (2000).
- ¹⁵L. A. Coldren and S. W. Corzine, *Diode Lasers and Photonic Integrated Circuits* (Wiley, New York, 1995).
- ¹⁶M. P. van Exter, A. K. J. van Doorn, and J. P. Woerdman, *Phys. Rev. A* **56**, 845 (1997).
- ¹⁷S. Ghosh, B. M. Arora, T. K. Sharma, and M. R. Gokhale, *J. Appl. Phys.* **83**, 5442 (1998).
- ¹⁸I. H. Campbell, T. W. Hagler, D. L. Smith, and J. P. Ferraris, *Phys. Rev. Lett.* **76**, 1900 (1996).
- ¹⁹E. Hecht, *Optics* (Addison-Wesley, Reading, 1998).